MATHEMATICAL BIOSCIENCES
AND ENGINEERING
Volume **1**, Number **2**, September **2004**

http://math.asu.edu/~mbe/

pp. **289–305**

A GENERAL MATHEMATICAL METHOD FOR INVESTIGATING THE THYMIC MICROENVIRONMENT, THYMOCYTE DEVELOPMENT, AND IMMUNOPATHOGENESIS

Guanyu Wang

Department of Pathology and laboratory Medicine,
The University of Texas Medical School at Houston
Houston, TX 77030

Gerhard R. F. Krueger

Department of Pathology and laboratory Medicine,
The University of Texas Medical School at Houston
Houston, TX 77030

(Communicated by Yang Kuang)

Abstract. T-lymphocyte (T-cell) development constitutes one of the basic and most vital processes in immunology. The process is profoundly affected by the thymic microenvironment, the dysregulation of which may be the pathogenesis or the etiology of some diseases. On the basis of a general conceptual framework, we have designed the first biophysical model to describe thymocyte development. The microclimate within the thymus, which is shaped by various cytokines, is first conceptualized into a growth field $\boldsymbol{\lambda}$ and a differentiation field $\boldsymbol{\mu}$, under the influence of which the thymocytes mature. A partial differential equation is then derived through the analysis of an infinitesimal element of the flow of thymocytes. A general method is presented to estimate the two fields based on experimental data obtained by flow cytometric analysis of the thymus. Numerical examples are given for both normal and pathologic conditions. Our results are quite good, and even the time varying fields can be accurately estimated. Our method has demonstrated its great potential for the study of immunopathogenesis. The plan for implementation of the method is addressed.

1. **Introduction.** T-lymphocytes perform a variety of important functions in immune regulation. Constant production of mature T-cells depends upon continuous seeding of the thymus by precursor cells from the bone marrow. The precursor cells are initially $CD3^-CD4^-CD8^-$ (triple negative [TN]) and can be divided on the basis of additional cell surface markers, such as CD44, CD25, and c-kit expressions. They mainly undergo T-cell receptor (TCR) gene rearrangement, rapidly followed by CD3, CD8, and CD4 expression, giving rise to the major pool of $CD4^+CD8^+$ (double positive [DP]) cells. Most DP cells express complete TCR-$\alpha\beta$ complexes, through which they receive signals for positive or negative selection. Positively selected cells then generate mature $CD4^+CD8^-$ or $CD4^-CD8^+$ single positive (SP) cells. For healthy adult mice, it has been estimated that it takes about 14 days to

2000 *Mathematics Subject Classification.* 92C50.

Key words and phrases. mathematical modeling, thymocyte development, T-cell immunology, immunopathogenesis, partial differential equations.

complete the TN stage [1, 2, 3], 3 to 4 days for the DP stage [4, 5], and 7 to 14 days for the SP stage [6, 7, 8]. The entire process entails a series of membranous events and interactions of cell membranes with cytokines and related substances that serve to communicate environmental influences to the cells. Such environmental signals serve to activate the respective genetic codes that modulate cellular reactions. Collectively, the cytokines, stroma cells, and other tissue factors, which provide the unique inductive role of the thymus, are termed the thymic microenvironment (T-MEV).

The impairment of T-MEV will result in the disturbances in the delicate network of cell proliferation and differentiation and finally will imbalance the system, resulting in pathologic over- or under-representation of certain parameters. This may result in clinical immunodeficiency or in progressive cell proliferation with ultimate tumor development, as demonstrated in early experiments [9-16]. The theory of dysregulative immunopathogenesis has been described in several previous publications [17-20] and was recently updated in a review paper [21]. According to this concept, diseases, such as malignant lymphomas, aplasias, or autoimmune disorders result from a disturbed balance of factors regulating cell differentiation, proliferation, and apoptosis. The theory does not contradict the current understanding of a genetic basis (e.g., transformation and atypia of specific cells) for many diseases. The genetic mutations may serve only as the etiology (causes) for some diseases, whose pathogenesis (development) depends heavily upon the immunologic regulations, or upon the T-MEV. The classic human example is infectious mononucleosis, where the Epstein-Barr virus does cause genetic mutations (just as in Burkitt's lymphoma), yet one gets no lymphomas because there is no sufficient deficiency in the immune system. Some evidences even suggest that the proliferation cells causing lymphomas need not be atypical transformed cells but may be just normal cells blocked in differentiation [18]. Therefore, immune dysregulation itself can lead to some diseases.

The original aim of this study is to elucidate quantitatively the influence of the T-MEV on the developing thymocytes, under physiologic and pathologic conditions. One would expect that a direct approach would be to measure the faculties of T-MEV: cell-cell interactions and cytokines. This, however, is impractical. Cell-cell interactions are difficult to measure and quantify. More than seventy cytokines and other tissue factors are known today [22], which in one way or another contribute to the proliferation and differentiation of thymocytes. Even if it were practical to measure all of them, their intensity distributions over the heterogeneous thymocytes can hardly be determined (as we will soon demonstrate, the geometries of the distributions are crucial to pathogenesis). Moreover, the intensity distribution corresponds poorly to the actual effect of a cytokine on thymocytes, since different thymocytes have different levels of expression of the cytokine receptor. To complicate matters, most cytokines have both effects of proliferation and differentiation, and it is impossible to decouple these by the cytokine measurements per se. Finally, the combined effect of all cytokines cannot simply be summed up from individual cytokine effects, because the action of cytokines are synergetic rather than additive [23]. The cytokines act in concert, but the synergetic mechanisms are unknown. All in all, these numerous, sporadic cytokines are very difficult to measure; their combined effect should be determined in some other way.

These difficulties force us to think of an alternative: Can we measure thymocytes instead? As products of the T-MEV, thymocytes must carry the information of the

T-MEV. That is, the immune regulation entailed in the thymocytes is encoded in the pattern of the thymic population distribution. It is thus possible to discern the T-MEV and to infer immunopathogenesis through decoding the thymocyte data. Mathematically, this kind of problem was termed the inverse problem [24]—determining unknown causes based on observations of their effects rather than by direct measurements of the causes. In this paper, the "cause" is summarized as thymocyte growth and differentiation functions, and a method is presented for determining them under physiologic and pathologic conditions.

Modeling of thymocyte development was first studied by Mehr et al. [25, 26, 27]. In their work, the temporal dynamics of four variables were simulated to represent four roughly divided thymic compartments (TN, DP, CD4+ SP, and CD8+ SP). However, the constituents of each compartment were undistinguishable, as they were represented together as a single variable. Restricted by its structure, Mehr et al.'s model has to modulate virtual effects of cytokines into only a few indirect coefficients. In reality, the cell distribution and the cytokine intensity distribution have rich geometries and great diversities that can be fully exposed only by a continuous model. In brief, their model, because it is a discrete (or multi-compartmental) one, is more suitable for tracking the macroscopic behavior of few discrete, roughly divided cell populations; the thymus as a whole still remains as a largely undefined black box. It is thus difficult to achieve our goal of revealing the diversity within the thymus to such an extent that the etiology and pathogenesis of some diseases can be elucidated.

Motions of continua, such as moving fluids and numerous other important phenomena, are better described by partial differential equations (PDEs). As a subphenomenon of hematopoiesis, which has been modeled by a PDE [28], thymopoiesis is more suitably modeled by a PDE. In this paper such a model is developed. A general method is also presented to determine the interactions between the developing thymocytes and the T-MEV, whereby the immunopathogenesis of some diseases is elucidated.

2. **Basic (physiologic) model.**

2.1. **Model design.** The whole cohort of thymocytes is considered in terms of a continuous flow (in contrast to the discrete compartments) through the thymus with ever-increasing maturity θ, originating as immature stem cells from the bone marrow and ending as mature T-cells. Upon this continuous flow, a growth field $\boldsymbol{\lambda}$ and a differentiation field $\boldsymbol{\mu}$ are imposed, representing the combined influences of all the cytokines (there are altogether about seventy effective cytokines in the thymus [22]). The steady-state distribution of the cell number, $\rho_0(\theta)$, is sustained by the two orthogonal fields (see Figure 1). The dynamical model is derived from the analysis of an infinitesimal element of the flow, $s = \rho(\theta, t)\, d\theta$, the growth of which is described by

$$\frac{\partial s}{\partial t} = \lambda(\theta)s + I - E \tag{1}$$

where

$$I = \rho(\theta, t)\mu(\theta) - \frac{\partial\left(\rho(\theta, t)\mu(\theta)\right)}{\partial\theta}\frac{d\theta}{2}$$

is the influx to s,

$$E = \rho(\theta,t)\mu(\theta) + \frac{\partial\left(\rho(\theta,t)\mu(\theta)\right)}{\partial\theta}\frac{d\theta}{2}$$

is the efflux from s, $\rho(\theta,t)$ is the cell number distribution with respect to θ at time t, $\mu(\theta) = \lim_{\Delta t\to 0} \Delta\theta/\Delta t$ is the differentiation field, $\lambda(\theta) = \lambda^p(\theta) - \lambda^a(\theta)$ is the growth field, $\lambda^p(\theta) = \lim_{\Delta t\to 0} \Delta p/(s\Delta t)$ is the proliferation rate (p is the cycling part of s), $\lambda^a(\theta) = \lim_{\Delta t\to 0} \Delta a/(s\Delta t)$ is the apoptosis rate (a is the dying part of s). Finally one obtains

$$\frac{\partial\rho(\theta,t)}{\partial t} + \frac{\partial\left(\rho(\theta,t)\mu(\theta)\right)}{\partial\theta} = \lambda(\theta)\rho(\theta,t) \tag{2}$$

with boundary conditions

$$\rho(0,t)\mu(0) = I_0,$$

where I_0 represents the number of cells entering the thymus in a unit of time (one day);

$$\lambda(0) = 0$$

(the progenitor cells enter the thymus at the cortico-medullary junction where few stimulating thymic epithelial cells reside [3]; the cell death is also negligible [29]).

Here, θ is defined as the maturity that a thymocyte of a healthy animal has so far achieved. It is quantitatively identified with the age of the cell (not the age of the animal), defined as the elapsed time after the cell has entered the thymus. For example, $\theta = 0$ represents the maturity of cells that are entering the thymus. These cells then mature and by day υ possess the maturity $\theta = \upsilon$. Following from the definition, the differentiation field for the healthy state is normalized and has the simple expression $\mu(\theta) = \lim_{\Delta t\to 0} \Delta\theta/\Delta t \equiv 1$ (the maturity gained in Δt days is quantitatively still Δt). Although θ is defined in terms of the healthy (physiologic) state, it can be used for pathologic conditions as well. In both cases, $\theta = \upsilon$ represents exactly the same level of maturation. However, for unhealthy animals the age of the thymocytes of maturity υ has the expression $t = \int_0^\upsilon d\theta/\mu(\theta)$, which does not necessarily equal υ, because $\mu(\theta) \equiv 1$ may not hold. One should bear in mind that maturity equals age only when the animal is healthy.

In what follows, we use the subscript 0 to denote quantities of the physiologic state. We have $\mu_0(\theta) \equiv 1$, and $\rho(\theta,t) = \rho_0(\theta)$, which is time invariant (the thymocytes are in homeostasis). Equation (2) then reduces to

$$\frac{d\rho_0(\theta)}{d\theta} = \lambda_0(\theta)\rho_0(\theta), \tag{3}$$

with $\rho_0(0) = I_0$, $\lambda_0(0) = 0$, which can be explicitly solved as

$$\rho_0(\theta) = I_0 \exp\left\{\int_0^\theta \lambda_0(\alpha)\, d\alpha\right\}. \tag{4}$$

The only unknown in Equation (3) is $\lambda_0(\theta)$. The following steps will obtain $\lambda_0(\theta)$.

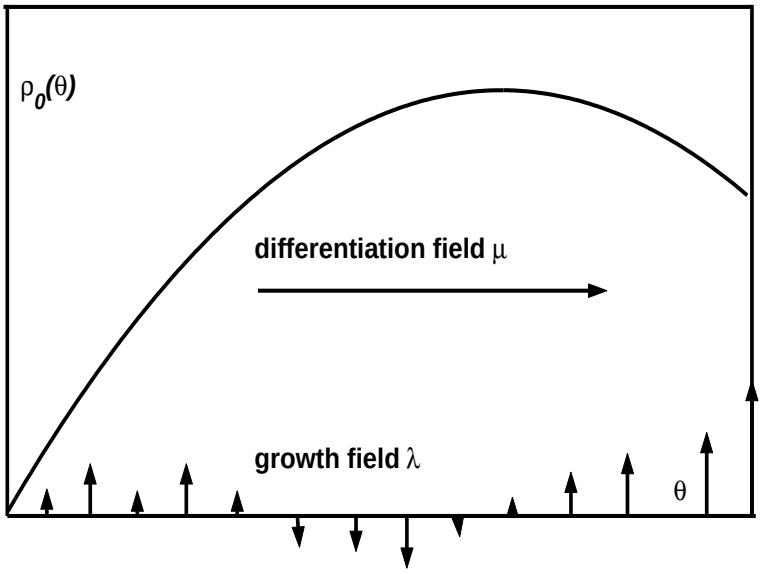

FIGURE 1. The steady-state distribution of thymocytes sustained by a growth field $\boldsymbol{\lambda}$ and a differentiation field $\boldsymbol{\mu}$.

2.2. **Experimental design.** Various cytokines shape $\lambda_0(\theta)$. To date these have been difficult to determine because of their large number. However, the thymocytes, upon which cytokines act, must carry the information of $\lambda_0(\theta)$. Therefore, $\lambda_0(\theta)$ can be determined from thymocytes on flow cytometric analysis. The flow cytometry is a specialized instrument that separates cell populations according to which florescent probe they bind to and the intensity of that binding. It also determines the cell number of each separated population [30]. After the thymus is harvested, thymocytes in suspension are sorted by flow cytometry into N sets, according to a given protocol of cell marker expression. The following three sets of data are then obtained:

1. Cell numbers of each set $\boldsymbol{S} = [S_1, S_2, \cdots, S_N]$ can be counted by the flow cytometry. S_i corresponds to the hatched area in Figure 2.
2. The mean proliferation rate of each set is as follows: $\overline{\boldsymbol{\lambda}}^p = \left[\overline{\lambda}_1^p, \overline{\lambda}_2^p, \cdots, \overline{\lambda}_N^p\right]$. Note that $\overline{\lambda}_i^p$ is the macroscopic version of the definition of λ^p (see Equation (1)). The number of cycling cells in set i, represented by P_i, can be obtained by flow cytometry that counts only the cycling cells that have been labeled by, for example, bromodeoxyuridine.
3. The mean apoptosis rate of each set is as follows: $\overline{\boldsymbol{\lambda}}^a = \left[\overline{\lambda}_1^a, \overline{\lambda}_2^a, \cdots, \overline{\lambda}_N^a\right]$. Note that $\overline{\lambda}_i^a$ is the macroscopic version of the definition of λ^a (see Equation (1)). The number of dying cells in set i, represented by A_i, can be obtained by flow cytometry that counts only the dying cells that have been stained by, for example, propidium iodide.

The data set is denoted by $\boldsymbol{d} = [\boldsymbol{S}, \overline{\boldsymbol{\lambda}}]^T$, where $\overline{\boldsymbol{\lambda}} = \overline{\boldsymbol{\lambda}}^p - \overline{\boldsymbol{\lambda}}^a$. There are in total $2N$ data.

It should be noted that although the limit definition of $\overline{\lambda}^p$ and $\overline{\lambda}^a$ may still seem too theoretical, in practice one can obtain them by taking advantages of other known biological facts, such as those present in Equations (11) and (12).

2.3. **Computation.** First, $\lambda_0(\theta) = \sum_{j=1}^{N} a_j f_j(\theta)$ is constructed in a space that is spanned by basis functions $f_j(\theta)$ $(j = 1, 2, \cdots, N)$, by which $\rho_0(\theta)$ has the expression

$$\rho_0(\theta) = I_0 \exp\left\{\sum_{j=1}^{N} a_j \int_0^{\theta} f_j(\alpha)\, d\alpha\right\}. \tag{5}$$

Whittaker's cardinal functions [31] $f_j(\theta) = \operatorname{sinc}(\pi(\theta - j\Delta)/\Delta)$ are chosen as the basis functions (Δ is the so-called Nyquist interval for which 3 is chosen in this section). By this choice, the boundary condition $\lambda_0(0) = 0$ automatically holds.

In the experimental design, the thymocytes have been divided into N sets. The delimitations between these sets are, however, unknown in terms of the defined maturity (although they are known in terms of cell-marker expression), which introduces N additional parameters $\boldsymbol{\theta} = [\theta_1, \theta_2, \cdots, \theta_N]^T$ (see Figure 2). Therefore, in total we have $2N$ unknowns $\boldsymbol{x} = [\boldsymbol{a}, \boldsymbol{\theta}]^T$, where $\boldsymbol{a} = [a_1, a_2, \cdots, a_N]^T$ is the representation of $\lambda_0(\theta)$. To relate the unknowns $\boldsymbol{x}$ to the data $\boldsymbol{b}$, the following $2N$ algebraic equations are established:

$$\int_0^{\theta_i} \rho_0(\theta)\, d\theta = \sum_{k=1}^{i} S_k, \text{ for } i = 1, 2, \cdots, N, \tag{6}$$

$$\int_{\theta_{i-1}}^{\theta_i} \lambda_0(\theta)\rho_0(\theta)\, d\theta = \overline{\lambda}_i S_i, \text{ for } i = 1, 2, \cdots, N. \tag{7}$$

Equation (6) is obvious. Equation (7) is identical with

$$\overline{\lambda}_i = \frac{\int_{\theta_{i-1}}^{\theta_i} \lambda_0(\theta)\rho_0(\theta)\, d\theta}{\int_{\theta_{i-1}}^{\theta_i} \rho_0(\theta)\, d\theta},$$

implying that the aggregately measured $\overline{\lambda}_i$ represents the growth rate averaged over all the cells in set i. By substituting Equation (3) into Equation (7), one iteratively obtains

$$R_i = I_0 + \sum_{k=1}^{i} \overline{\lambda}_k S_k, \text{ for } i = 1, 2, \cdots, N, \tag{8}$$

where R_i denotes $\rho_0(\theta_i)$ (see Figure 2). By replacing θ with θ_i in Equation (5), one obtains

$$\sum_{j=1}^{N} a_j \int_0^{\theta_i} f_j(\alpha)\, d\alpha - \ln(R_i/I_0) = 0, \text{ for } i = 1, 2, \cdots, N. \tag{9}$$

Substituting Equation (5) into Equation (6),

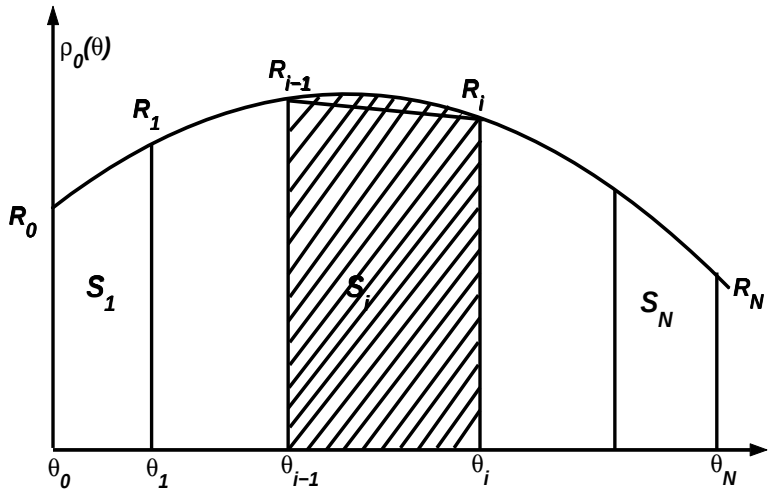

FIGURE 2. An illustration of parameters $\boldsymbol{\theta}, \boldsymbol{R}$, and $\boldsymbol{S}$. $\boldsymbol{\theta} = [\theta_0, \theta_1, \cdots, \theta_N]$ is the set of delimitations between sets. $\boldsymbol{R} = [R_0, R_1, \cdots, R_N]$, where R_i represents $\rho_0(\theta_i)$. $\boldsymbol{S} = [S_0, S_1, \cdots, S_N]$, where S_i is the cell number of set i and equals the hatched area.

$$I_0 \int_0^{\theta_i} \exp\left(\sum_{j=1}^{N} a_j \int_0^{\theta_i} f_j(\alpha)\, d\alpha\right) d\theta - \sum_{k=1}^{i} S_k, \text{ for } i = 1, 2, \cdots, N. \tag{10}$$

Equations (9) and (10) will be used to obtain $\mathbf{x}$ by applying Newton's method [32], a standard root-finding method. The method operates iteratively and requires that the initial value be sufficiently close to the actual solution; otherwise, the convergence would be difficult to reach, especially for the present high-dimensional case. A preliminary calculation is therefore necessary to localize the approximate solution.

FIRST APPROXIMATION. From Figure 2, one sees that S_i (hatched area) approximately equals the trapezoid $\theta_{i-1}\theta_i R_i R_{i-1}$, namely $(\theta_i - \theta_{i-1})(R_i + R_{i-1})/2 \approx S_i$. Therefore, the approximated value $\boldsymbol{\theta}^{(0)}$ can be obtained according to $\theta_i^{(0)} = \theta_{i-1}^{(0)} + 2S_i/(R_{i-1} + R_i)$. Subsequently $\boldsymbol{a}^{(0)}$ can be obtained from Equation (9), namely, $\boldsymbol{a} = \boldsymbol{Q}^{-1}\boldsymbol{e}$, where $\boldsymbol{e} = [\ln(R_1/I_0), \cdots, \ln(R_N/I_0)]^T$, and $\boldsymbol{Q}$ is a $N \times N$ matrix, with $Q_{ij} = \int_0^{\theta_i} f_j(\alpha)\, d\alpha$.

ROOT FINDING. The obtained $\boldsymbol{x}^{(0)} = [\boldsymbol{a}^{(0)}, \boldsymbol{\theta}^{(0)}]^T$ is used as the initial value for finding the root of Equations (9) and (10) (denoted by $F(\boldsymbol{x}) = 0$ hereinafter). Newton's method is as follows:

Given $\boldsymbol{x}^{(0)}$, for $k = 0, 1, \cdots$, until convergence:
Solve: $J_F(\boldsymbol{x}^{(k)})\delta\boldsymbol{x}^{(k)} = F(\boldsymbol{x}^{(k)})$,
Set: $\boldsymbol{x}^{(k+1)} = \boldsymbol{x}^{(k)} - \delta\boldsymbol{x}^{(k)}$,

where

$$J_F(\boldsymbol{x}) = \begin{bmatrix} \boldsymbol{Q} & \boldsymbol{L} \\ \boldsymbol{M} & \boldsymbol{R} \end{bmatrix}$$

is the Jacobian matrix associated with $F(\boldsymbol{x})$, $\boldsymbol{L} = \text{diag}\{\lambda(\theta_1), \lambda(\theta_2), \cdots, \lambda(\theta_N)\}$, $\boldsymbol{M}$ is a $N \times N$ matrix with $M_{ij} = \int_0^{\theta_i} \rho_0(\theta) \int_0^{\theta} f_j(\alpha)\, d\alpha\, d\theta$, and $\boldsymbol{R} = \text{diag}\{R_1, R_2, \cdots, R_N\}$.

The computation of $\boldsymbol{\theta}$ is also a process of calibration, by which the relation is found between the theoretical maturity $\boldsymbol{\theta}$ and the practical maturity (cell marker expressions) used to demarcate the cells in the experiment. In future studies, if the same $\boldsymbol{\theta}$ values are used for computation, the same protocol must be used in the experiment.

2.4. **Numerical example.** To give an example, we performed an extensive literature survey and found only one set of data [33] that appears sufficient. The data were obtained from a healthy mouse and described only the TN stage. TN thymocytes were divided into $N = 6$ sets, namely, $\text{CD44}^+\text{CD25}^-$ (TN_1), $\text{CD44}^+\text{CD25}^{low}$ (TN_2), $\text{CD44}^+\text{CD25}^{high}$ (TN_3), $\text{CD44}^-\text{CD25}^{high}$ (TN_4), $\text{CD44}^-\text{CD25}^{low}$ (TN_5), and $\text{CD44}^-\text{CD25}^-$ (TN_6). The cell numbers of each set, $\boldsymbol{S} = [S_1, S_2, \cdots, S_6]$, are given. Instead of obtaining the proliferation rate $\overline{\lambda}_i^p$ ($i = 1, 2, \cdots, 6$), these authors measured the labeling index α_i, that is, the percentage of the cycling cells in set i ($\alpha_i = P_i/S_i$). Fortunately, $\overline{\lambda}_i^p$ can be derived from α_i, namely,

$$\overline{\lambda}_i^p = \lim_{\Delta t \to 0} \frac{\Delta P_i}{S_i \Delta t} = \frac{P_i}{S_i} \lim_{\Delta t \to 0} \frac{\Delta P_i}{P_i \Delta t} = \alpha_i \kappa, \tag{11}$$

where

$$\kappa = \lim_{\Delta t \to 0} \frac{\Delta P_i}{P_i \Delta t}. \tag{12}$$

Another version of Equation (12) is $\dot{P}_i = \kappa P_i$, by which κ is deduced as $\ln 2/T$, where T is the cycle time (the time required for cell doubling). For the great majority of the cycling thymocytes, T is about 9 to10 hours [34]. We use $T =$ 9.5 hours $= 0.39583$ days , whereby $\kappa = 1.7511/$ day is obtained. The rates of apoptosis $\overline{\lambda}_i^a$ ($i = 1, 2, \cdots, 6$) are not provided in [33]. However, the TN stage is characterized by extensive expansion [35], and the apoptosis rate is much less than the proliferation rate. Some studies (e.g., [29]) have shown that the baseline apoptosis level of the TN cells is indeed very low and can be ignored. However, at the $\text{CD44}^-\text{CD25}^{high}$ (TN_4) stage, where the TCR β-selection takes place, apoptosis was considerable and was estimated to be about 70 % of the corresponding proliferation [33] or $\overline{\lambda}_4^a \approx 0.7\overline{\lambda}_4^p$. Other $\overline{\lambda}_i^a$ values ($i = 1, 2, 3, 5, 6$) are simply assumed as 0. For the present case of a normal, unmanipulated thymus, I_0 was estimated to be between 5×10^4 per day and 5×10^5 per day [34].

Following computation using a trial value $I_0 = 5 \times 10^4$ per day, $\boldsymbol{x} = [\boldsymbol{a}, \boldsymbol{\theta}]$ is obtained. In particular, the value of θ_6 (represents the length of the TN stage) is 18.06— that is, close to 14, the generally accepted value [1, 2, 3]. By repetition of the computation using a larger I_0, θ_6 can be accurately tuned to 14. The final result is as follows: $I_0 = 8.075 \times 10^4$ per day, $\boldsymbol{a} = [0.0622, 0.367, 0.250, -0.276, 0.641, 0.177]$, $\boldsymbol{\theta} = [4.203, 4.768, 6.078, 12.324, 13.481, 14.000]$. Figure 3 shows the obtained $\lambda_0(\theta)$, $\rho_0(\theta)$ and the profile of the CD44 and CD25 expressions, where $\boldsymbol{\theta}$ are shown as the dotted lines. TN_4 is the longest, which implies that some complex process may be involved. Indeed, at this stage most of the cells display the hallmark of irreversible immunological commitment to the T lineage in the form of TCR β-gene rearrangements [3, 33]. The process may generate out-of-frame TCR β-chains that are unresponsive to stimulation; cells carrying such pre-TCR will subsequently die.

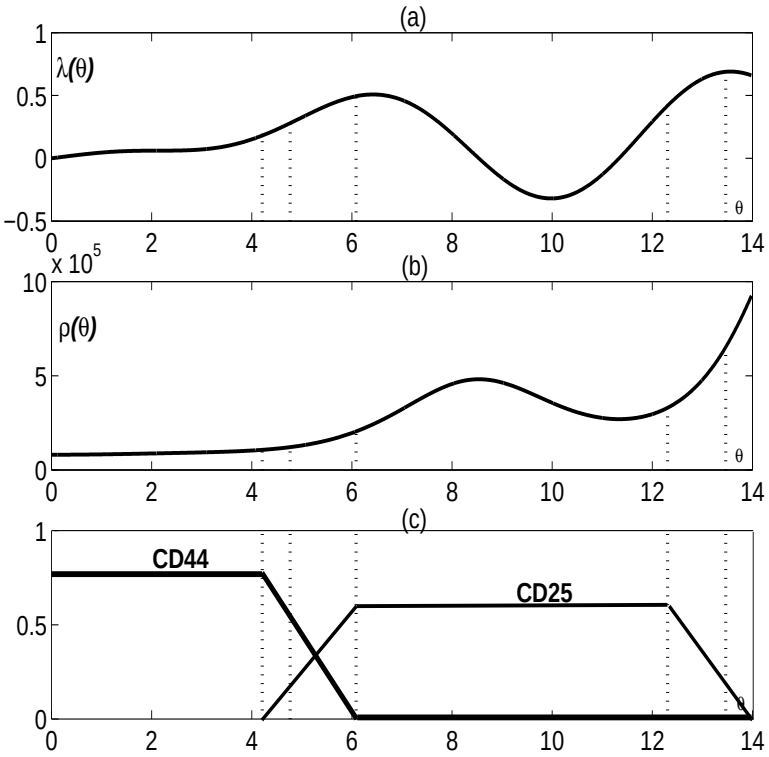

FIGURE 3. Results of the base model. Figures a and b show $\lambda_0(\theta)$ and $\rho_0(\theta)$, obtained with $I_0 = 8.075 \times 10^4$. Figure c shows the expression profile of CD44 (thick line) and CD25 (thin line). The dotted lines show the delimitations between sets.

This may well be the reason why $\lambda_0(\theta)$ has a negative part in the TN_4 stage as shown in Figure 3a. Note that $\rho_0(\theta)\mu_0(\theta)$ has the physical meaning of the number of cells passing through θ in a unit of time. As a benefit of our definition of θ, this term reduces to $\rho_0(\theta)$ and can be read directly from Figure 3b. For example, one reads that each day 3×10^5 cells leave TN_3 and enter TN_4, and 9.05×10^5 cells per day leave the TN stage. From Figure 3c, one sees that upregulation and downregulation of CD44 and CD25 are fast processes, as indicated by the short periods of the $TN_{2,3,5,6}$ stages.

3. **Disturbed (pathologic) model I.** Consider an abrupt disturbance of the two fields in the thymus, namely, change $\lambda_0(\theta), \mu_0(\theta)$ to some unknown, time-invarying $\tilde{\lambda}(\theta), \tilde{\mu}(\theta)$. As a consequence, the density distribution $\rho(\theta, t)$ gradually drifts from the initial $\rho_0(\theta)$ according to

$$\frac{\partial \rho(\theta,t)}{\partial t} + \frac{\partial \left(\rho(\theta,t)\tilde{\mu}(\theta)\right)}{\partial \theta} = \tilde{\lambda}(\theta)\rho(\theta,t), \tag{13}$$

with the (left) boundary conditions $\rho(0,t) = I_0, \tilde{\lambda}(0) = 0$, and $\tilde{\mu}(0) = 1$ (the disturbance is assumed to occur only within the thymus, which will not alter the left

boundary), until a new equilibrium $\tilde{\rho}(\theta)$ is reached. In that case, $\tilde{\rho}(\theta)$ is governed by

$$\frac{d\left(\tilde{\rho}(\theta)\tilde{\mu}(\theta)\right)}{d\theta} = \tilde{\lambda}(\theta)\tilde{\rho}(\theta). \tag{14}$$

At the new equilibrium, the thymus is harvested, the suspended thymocytes are divided into N sets according to the same protocol of cell-marker expression as the normal study, and the data $\boldsymbol{d} = [\boldsymbol{S}, \overline{\boldsymbol{\lambda}}]^T$ are obtained by flow cytometric analysis. Now the problem is how to determine the unknown $\tilde{\lambda}(\theta)$ and $\tilde{\mu}(\theta)$ based on the obtained data $\boldsymbol{d}$. Since$\boldsymbol{\theta}$ values have already been obtained in the normal study, the $2N$ data can be used exclusively to obtain $\tilde{\lambda}(\theta)$ and $\tilde{\mu}(\theta)$ through

$$\int_0^{\theta_i} \tilde{\rho}(\theta)\, d\theta = \sum_{k=1}^{i} S_k, \text{ for } i = 1, 2, \cdots, N, \tag{15}$$

$$\int_{\theta_{i-1}}^{\theta_i} \tilde{\lambda}(\theta)\tilde{\rho}(\theta)\, d\theta = \overline{\lambda}_i S_i, \text{ for } i = 1, 2, \cdots, N. \tag{16}$$

For the sake of easy computation, we let

$$\frac{\tilde{\lambda}(\theta)}{\tilde{\mu}(\theta)} = \sum_{j=1}^{N} b_j f_j(\theta)$$

and

$$\frac{1}{\tilde{\mu}(\theta)} = 1 + \sum_{j=1}^{N} c_j f_j(\theta);$$

1 must be added to satisfy the boundary condition $1/\tilde{\mu}(0) = 1$. The $2N$ unknowns are thus $\boldsymbol{x} = [\boldsymbol{b}, \boldsymbol{c}]^T$. By substituting Equation (14) into Equation (16), one obtains

$$\tilde{R}_i = I_0 + \sum_{k=1}^{i} \overline{\lambda}_k S_k, \text{ for } i = 1, 2, \cdots, N, \tag{17}$$

where $\tilde{R}_i$ represents $\tilde{\rho}_0(\theta_i)\tilde{\mu}_0(\theta_i)$. On the other hand, from Equation (14),

$$\tilde{\rho}(\theta)\tilde{\mu}(\theta) = I_0 \exp\left(\int_0^{\theta} \frac{\lambda(\alpha)}{\mu(\alpha)}\, d\alpha\right) = I_0 \exp\left(\sum_{j=1}^{N} b_j \int_0^{\theta} f_j(\alpha)\, d\alpha\right). \tag{18}$$

Associating Equation (18) with (17) by replacing θ with θ_i, one obtains

$$\sum_{j=1}^{N} b_j \int_0^{\theta_i} f_j(\alpha)\, d\alpha - \ln(\tilde{R}_i/I_0) = 0, \text{ for } i = 1, 2, \cdots, N. \tag{19}$$

Then, $\boldsymbol{b} = \boldsymbol{Q}^{-1}\boldsymbol{e}$ is readily obtained, where $\boldsymbol{e} = [\ln(\tilde{R}_1/I_0), \cdots, \ln(\tilde{R}_N/I_0)]^T$, and $\boldsymbol{Q}$ is as before. From Equation (18) one has

$$\tilde{\rho}(\theta) = \frac{\varphi(\theta)}{\tilde{\mu}(\theta)} = \varphi(\theta)\left(1 + \sum_{j=1}^{N} c_j f_j(\theta)\right), \tag{20}$$

where $\varphi(\theta) = I_0 \exp\left(\sum_{j=1}^{N} b_j \int_0^{\theta} f_j(\alpha)\, d\alpha\right)$ is a known function now. Substituting Equation (20) into Equation (15), one obtains

$$\boldsymbol{c} = \boldsymbol{\Psi}^{-1}\boldsymbol{l}, \tag{21}$$

where $\boldsymbol{\Psi}$ is a $N \times N$ matrix with $\Psi_{ij} = \int_0^{\theta_i} f_j(\theta)\varphi(\theta)\, d\theta$, $\boldsymbol{l} = [l_1, \cdots, l_i, \cdots, l_N]^T$ with $l_i = \sum_{k=1}^{i} S_k - \int_0^{\theta_i} \varphi(\theta)\, d\theta$. One subsequently obtains

$$\tilde{\mu}(\theta) = \frac{1}{1 + \sum_{j=1}^{N} c_j f_j(\theta)},$$

$$\tilde{\lambda}(\theta) = \frac{\sum_{j=1}^{N} b_j f_j(\theta)}{1 + \sum_{j=1}^{N} c_j f_j(\theta)},$$

$$\tilde{\rho}(\theta) = \frac{\varphi(\theta)}{\tilde{\mu}(\theta)}.$$

3.1. **Numerical examples.** Example I. The perturbed fields $\tilde{\lambda}(\theta)$ and $\tilde{\mu}(\theta)$ are prescribed and are shown as solid lines in Figure 4a and 4b in comparison to the normal fields (dotted lines). The general tendency of the prescribed fields mimics actual pathological conditions [12, 18]. Since no real experiment is available, the following simulated experiment is performed to obtain the data set $\boldsymbol{d} = [\boldsymbol{S}, \overline{\boldsymbol{\lambda}}]^T$.

Equation (13) is first integrated to obtain $\rho(\theta, t)$, which simulates the real cell evolution. The result is shown in Figures 4c and 4d. One sees that at $t = 20$ (days) the steady state $\tilde{\rho}(\theta)$ has been reached. The θ-axis is divided into N parts with $\theta_i = 14i/N$, where $i = 1, 2, \cdots, N$. One then calculates $\boldsymbol{S}$ and $\overline{\boldsymbol{\lambda}}$ according to $S_i = \int_{\theta_{i-1}}^{\theta_i} \tilde{\rho}(\theta)\, d\theta$ and $\overline{\lambda}_i = \int_{\theta_{i-1}}^{\theta_i} \tilde{\lambda}(\theta)\tilde{\rho}(\theta)\, d\theta / \int_{\theta_{i-1}}^{\theta_i} \tilde{\rho}(\theta)\, d\theta$.

Based on the data $\boldsymbol{d} = [\boldsymbol{S}, \overline{\boldsymbol{\lambda}}]^T$ only, we now test our method of estimating $\tilde{\lambda}(\theta)$ and $\tilde{\mu}(\theta)$, to see if the reconstructed ones mimic the prescribed ones. The parameters $\boldsymbol{b}$ and $\boldsymbol{c}$ are computed according to Equations (19) and (21) (for the Nyquist interval, $\Delta = 14/N$ is chosen). The reconstructed $\tilde{\mu}(\theta), \tilde{\lambda}(\theta)$, and $\tilde{\rho}(\theta)$ are shown in Figure 4e and 4f. Different colors represent different values of N. One sees that all the reconstructions are accurate. The accuracy improves as N increases.

Example II.The example is shown in Figure 5. One sees that the reconstructions are also accurate. For $N = 6$, the reconstruction is not as good near the peaks around $\theta = 3$. Fortunately as N increases, the reconstruction does become accurate.

4. **Disturbed (pathologic) model II.** In this section, we consider the gradual, slow changes $\lambda(\theta, t)$ and $\mu(\theta, t)$ that drive the evolution of $\rho(\theta, t)$ according to

$$\frac{\partial \rho(\theta, t)}{\partial t} + \frac{\partial \left(\rho(\theta, t)\mu(\theta, t)\right)}{\partial \theta} = \lambda(\theta, t)\rho(\theta, t), \tag{22}$$

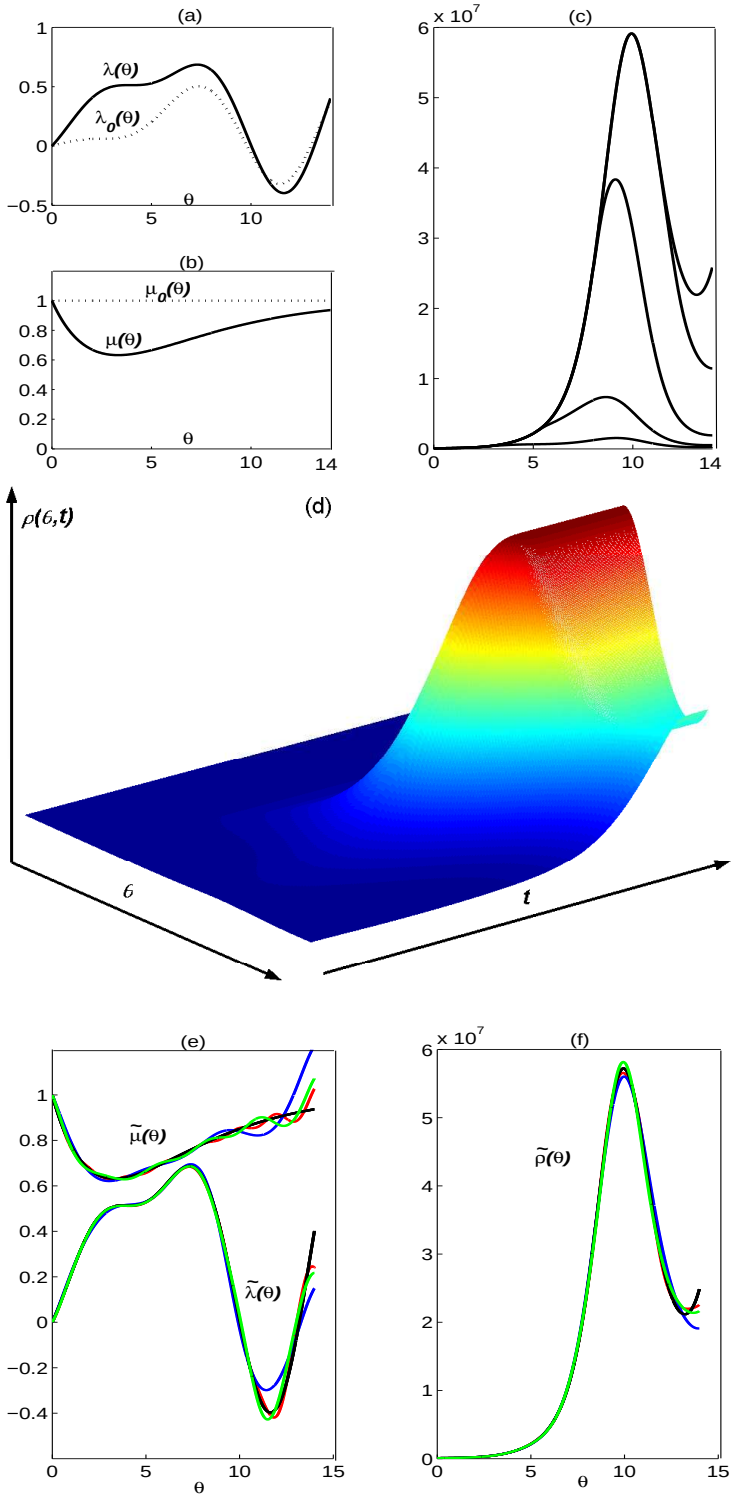

FIGURE 4. Example 1 of the disturbed model I. (a, b) The disturbed fields $\tilde{\mu}(\theta)$ and $\tilde{\lambda}(\theta)$ (solid lines) in comparison to the normal fields (dotted lines). (c) The evolution $\rho(\theta, t)$ sampled at discrete times $t = 4, 8, 12, 16, 20$ days. (d) The entire $\rho(\theta, t)$ begins as $\rho_0(\theta)$ and ends at $t = 20$. (e, f) The reconstructed $\tilde{\mu}(\theta)$ and $\tilde{\lambda}(\theta)$ in comparison to the original ones (in black). Blue, green, and red lines represent results obtained with $N = 6, 10,$ and 14, respectively.

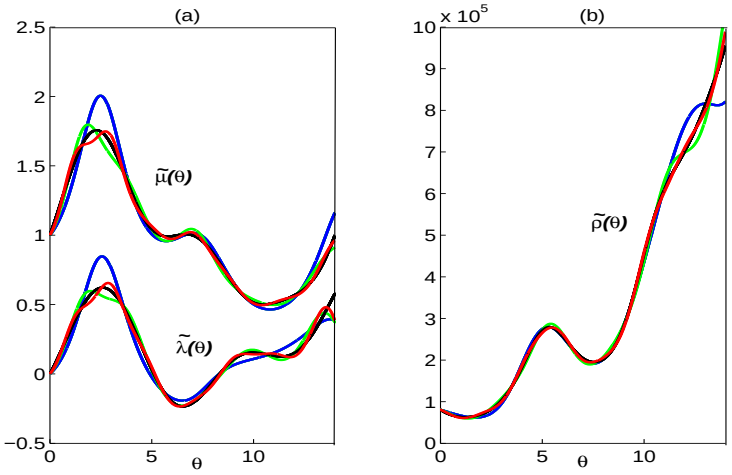

FIGURE 5. Example 2 of the disturbed model I. The reconstructed $\tilde{\mu}(\theta)$ and $\tilde{\lambda}(\theta)$ in (a) and $\tilde{\rho}(\theta)$ in (b) are shown in color and compared with the original ones (in black). The blue, green, and red lines represent the results obtained with $N = 6, 10$, and 14, respectively.

with initial conditions $\rho(\theta, 0) = \rho_0(\theta), \lambda(\theta, 0) = \lambda_0(\theta), \mu(\theta, 0) = \mu_0(\theta)$, and boundary conditions $\rho(0, t) = I_0, \lambda(0, t) = 0, \mu(0, t) = 1$. In this case, a steady state will never be reached, since the driving forces always vary with time. However, if $\lambda(\theta, t)$ and $\mu(\theta, t)$ change slowly, the process is in the quasi-steady state $\partial\rho(\theta, t)/\partial t \approx 0$, which means that at any time τ the system state is approximately steady, and the method of the last section can still be used to estimate $\lambda(\theta, \tau)$ and $\mu(\theta, \tau)$.

Model 2 is more practical than model 1, since a fixed thymic microenvironment is unlikely under pathologic conditions. Generally, the microenvironment drifts slowly from normal (e.g., as caused by viral infection), which also drives diseases slowly.

4.1. **Numerical examples.** The results of three examples (denoted by subscripts 1, 2, and 3) are shown in the left, middle and right columns of Figure 6. The only differences among the examples are the change rates of $\xi(\theta, t)$ ($\xi = \lambda$ and μ): example 3 is two times faster than example 2 and six times faster than example 1 ($\partial\xi_3/\partial t = 2\partial\xi_2/\partial t = 6\partial\xi_1/\partial t$).

By integrating Equation (22) with prescribed fields $\lambda(\theta, t)$ and $\mu(\theta, t)$, the evolution $\rho(\theta, t)$ is first obtained. We estimate the varying fields at certain times $t_k (k = 1, 2, \cdots)$, typically multiples of 100. At these times the data $\boldsymbol{d}(t_k) = [\boldsymbol{S}(t_k), \overline{\boldsymbol{\lambda}}(t_k)]^T$ are generated according to

$$S_i(t_k) = \int_{\theta_{i-1}}^{\theta_i} \rho(\theta, t_k)\, d\theta,$$

$$\overline{\lambda}_i(t_k) = \frac{\int_{\theta_{i-1}}^{\theta_i} \lambda(\theta, t_k)\rho(\theta, t_k)\, d\theta}{\int_{\theta_{i-1}}^{\theta_i} \rho(\theta, t_k)\, d\theta},$$

$$\text{for } i = 1, 2, \cdots, N = 20.$$

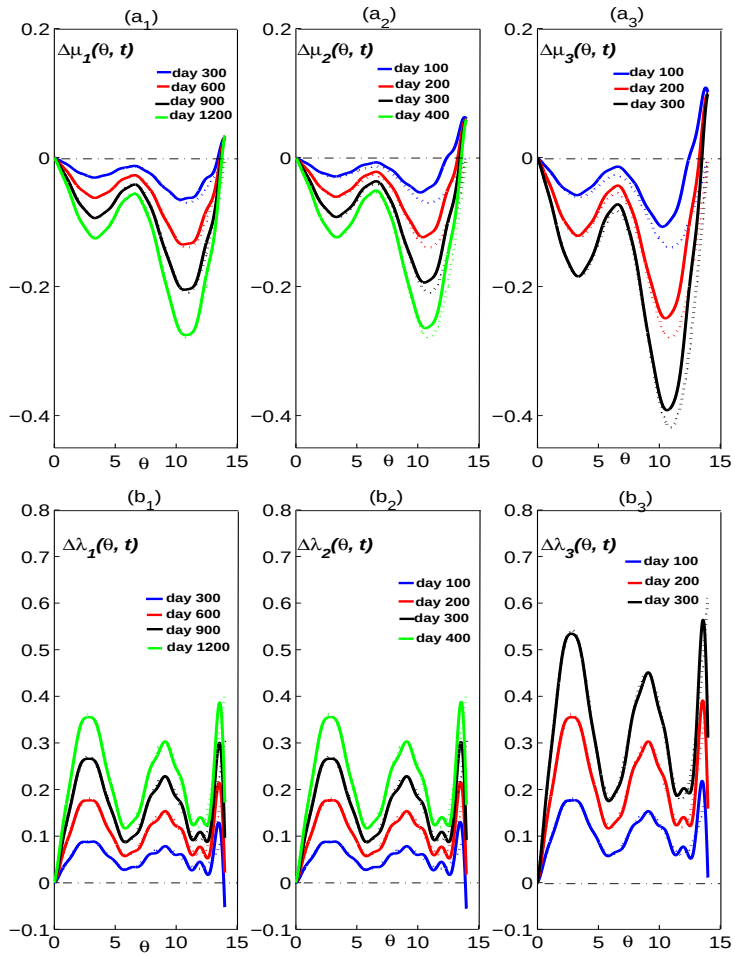

FIGURE 6. Results of the disturbed model II. $(a_i,\ b_i)$ show $\Delta\mu(\theta, t_k)$ and $\Delta\lambda(\theta, t_k)$ of example $i (i = 1, 2, 3)$. The dash-dotted line is the zero-reference. The dotted (solid) lines are for the prescribed (reconstructed) values. Different colors represent different t_k values, as defined in the legends.

With these data, the parameters $\boldsymbol{b}(t_k), \boldsymbol{c}(t_k)$ are computed, and $\lambda(\theta, t_k), \mu(\theta, t_k)$ and $\rho(\theta, t_k)$ are reconstructed.

For a clear illustration we show in Figure 6

$$\Delta\mu(\theta, t_k) = \mu(\theta, t_k) - \mu_0(\theta)$$

and

$$\Delta\lambda(\theta, t_k) = \lambda(\theta, t_k) - \lambda_0(\theta)$$

instead of $\mu(\theta, t_k)$ and $\lambda(\theta, t_k)$ themselves. The dotted (solid) lines represent the prescribed (reconstructed) values. One sees that the reconstructions are quite accurate despite the fact that the system states are not strictly steady. The error of example 3 is larger than those of examples 1 and 2, implying that the performance degrades as the fields change faster.

5. **Discussion.** T-cell development constitutes one of the basic and most vital processes in immunology, the modeling of which is naturally of great significance. A good conceptual framework is essential to reducing the enormously complicated process to a realistic biophysical model that can provide insights leading to new theory and discovery. In this article such a framework has been presented. The key idea is the conceptualization of the microclimate (shaped by various cytokines) within the thymus into two fields $\boldsymbol{\lambda}$ (growth) and $\boldsymbol{\mu}$ (differentiation), which drive the thymocyte development from different directions. The model has been fully analyzed, and a method of estimating the two fields has been developed. The method can accurately estimate variational fields, provided that they do not vary too fast.

Although based mostly on simulated data, the study still has great practical significance. On one hand, these simulated data have definite physical meanings and are experimentally viable. On the other hand, the simulation study is a necessary step to validate the method. Practically speaking, one cannot tell whether or not the estimations are accurate, since no comparisons are available. In the simulation study, the direct comparisons between the prescribed fields and the reconstructed ones demonstrate the accuracy and the potential of the method in estimating the real thymic microenvironment.

Suppose one is to study a diseased mouse. The following two-step procedure is proposed:

Step 1. Use a healthy mouse for calibration and comparison. Its thymocytes are sorted into N sets based on the expressions of some chosen cell markers (represented by the fluorescence intensity values in flow cytometric analysis). After data collecting and computation, $\boldsymbol{x} = [\boldsymbol{a}, \boldsymbol{\theta}]$ is obtained. From $\boldsymbol{a} = [a_1, a_2, \cdots, a_N]$, $\lambda_0(\theta)$ is constructed from and shall be used for comparison. For the computation in step 2, $\boldsymbol{\theta} = [\theta_1, \theta_2, \cdots, \theta_N]$ shall be used.

Step 2. Now the diseased mouse is studied. The same criteria as in step 1 is used to divide the cells into N sets in the experiment; the same $\boldsymbol{\theta} = [\theta_1, \theta_2, \cdots, \theta_N]$ as in step 1 is employed in Equations (19) and (21) to obtain $\boldsymbol{b}$ and $\boldsymbol{c}$. The disturbed fields and the cell distribution are subsequently constructed.

Because of its commonality, step 1 should be standardized to avoid repeated labors. A protocol should be carefully designed for cell pool division. By using a large N, a very detailed landscape of the thymus can be obtained.

Suppose the TN part of the estimated fields are shown in Figures $6a_1$ and $6b_1$. By comparison with $\lambda_0(\theta)$ and $\mu_0(\theta)$, one immediately finds that the cells have an elevated proliferation; the differentiation slows throughout the range, with the severest block at $\theta = 10.8$. Noticing that $\theta = 10.8$ is within some set defined by, for example, $0 < \mathrm{CD44} < 10$, $200 < \mathrm{CD25} < 250$, one determines that the differentiation is mostly blocked at these particular cells. Apparently, a larger N implies a better resolution. By viewing on a computer screen the movie of the two fields drifting away from the normal ones, the etiology and pathogenesis of the disease can be elucidated vividly. Without the theory, such detailed quantitative conclusions can hardly be drawn; even the cell distribution $\rho(\theta)$ cannot be obtained. Indeed, the raw data from the experiment are only discrete numbers.

Various publications of T-cell changes following cellular differentiation blocks after oncogenic viral infection or chemical carcinogenesis indicate that the model presented here can actually simulate known pathologic processes. Blocks in thymic differentiation were demonstrated in mouse lymphomas induced by Grossvirus,

Moloneyvirus, and nitrosobutylurea [11, 13, 14] and in the human T-cell proliferative disorders Canale-Smith syndrome and HTLV-1 infection [36, 37]. By using the present method, it is possible that in the future the etiology and the pathogenesis of these diseases can be quantitatively characterized. The present model thus appears to be a valuable tool for studying immunopathogenesis, including lymphoma development.

Acknowledgments. We thank Dr. L. Maximilian Buja for his support and technical advices.

REFERENCES

[1] K. Shortman, M. Egerton, G. Spangrude, and R. Scollary, "The generation and fate of thymocytes," Semin. Immunol., vol. 2, pp. 3–12, 1990.

[2] C. Benoist and D. Mathis, "T-lymphocyte differentiation and biology," in FUNDAMENTAL IMMUNOLOGY, 4 ed., ed. W. Pau. Lippincott-Raven, Philadelphia, 1999, pp. 367–409.

[3] H. Petrie, "Role of thymic organ structure and stromal composition in steady-state postnatal T-cell production," Immunol. Rev., vol. 189, pp. 8–19, 2002.

[4] M. Egerton, R. Scollay, and K. Shortman, "Kinetics of mature T-cell development in the thymus," PNAS, vol. 97, pp. 2579–2582, 1990.

[5] M. Huesmann, B. Scott, P. Lisielow, and H. von Boehmer, "Kinetics and efficacy of T-cell positive selection in thymus of normal and T-cell receptor transgenic mice," Cell, vol. 66, pp. 533–540, 1991.

[6] R. Scollay and D. I. Godfrey, "Thymic emigration: Conveyor belts or lucky dips?" Immunol. Today, vol. 16, pp. 268–273, 1995.

[7] D. Tough and J. Sprent, "Thymic emigration-a reply," Immunol. Today, vol. 16, pp. 273–274, 1995.

[8] R. Rooke, C. Waltzinger, C. Benoist, and D. Mathis, "Targeted complementation of MHC class II deficiency by intrathymic delivery of recombinant adenoviruses," Immunity, vol. 7, pp. 123–134, 1997.

[9] G. Krueger, R. Malmgren, and C. Berard, "Malignant lymphomas and plasmacytosis in mice under chronic immunosuppression and persistent antigenic stimulation," Transplantation, vol. 11, pp. 128–144, 1971.

[10] G. Krueger, "Chronic immunosuppression and lymphomagenesis in man and mice," Ntl Cancer Int Monogr, vol. 35, pp. 183–190, 1972.

[11] G. Krueger, R. Fischer, and H. Flesch, "Sequential changes in T- and B-cells, virus antigen expression and primary histologic diagnosis in virus-induced lymphomagenesis in mice," Z. Krebsforsch, vol. 92, pp. 41–54, 1979.

[12] G. Krueger, A. Karpinski, U. Heine, and B. Koch, "Differentiation block of prethymic lymphocytes during Moloneyvirus induced lymphoma development associated with a thymic epitheliel defect," J Cancer Res Clin Oncol, vol. 106, pp. 153–157, 1983.

[13] M. Kraus and G. Krueger, "T- and B-cell determination in various lymphoid tissues of mice during N-nitrosobutylurea (NBU) leukemogenesis," J Cancer Res Clin Oncol, vol. 100, pp. 149–165, 1981.

[14] U. Heine, G. Krueger, A. Karpinski, E. Munoz, and M. Krueger, "Quantitative light and electron microscopic changes in thymic reticular epithelial cells during Moloneyvirus induced lymphoma development," J Cancer Res Clin Oncol, vol. 106, pp. 102–111, 1983.

[15] S. Daefler and G. Krueger, "Expression of proliferation and differentiation antigens in response to modulation of membrane lipid fluidity in chronic lymphatic leukemia lymphocytes," Anticancer Res, vol. 9, pp. 501–506, 1989.

[16] S. Daefler and G. Krueger, "Lack of dynamic lipid changes after binding of interleukin-2 in chronic lymphocytis leukemia lymphocytes indicates defective transmembrane signaling," Anticancer Res, vol. 9, pp. 743–748, 1989.

[17] D. Purtilo, E. Tatsumi, G. Manolov, Y. Manolova, S. Harada, H. Lipscomb, and G. Krueger, "Epstein-Barr virus as an etiological agent in the pathogenesis of lymphoproliferative and aproliferative diseases in immune deficient patients," Int Rev Exp Path, vol. 27, pp. 113–183, 1985.

[18] G. Krueger, "Abnormal variation of the immune system as related to cancer," in Cancer Growth and Progression, H. Kaiser, Ed. Dordrecht NL: Kluwer Acad Publ, 1989, pp. 139–161.

[19] M. Schonnebeck, G. Krueger, M. Braun, M. Fischer, B. Koch, D. Ablashi, and N. Balachandran, "Human herpesvirus-6 infection may predispose cells for superinfection by other viruses," In Vivo, vol. 5, pp. 255–264, 1991.

[20] G. Krueger and A. V. Ferrer, "A unifying concept of viral immunopathogeneis of proliferative and aproliferative diseases (working hypothesis)," In Vivo, vol. 8, pp. 493-500, 1994.

[21] G. Krueger, A. Nguyen, M. Uthman, M. Brandt, and L. Buja, "Dysregulative lymphoma theory revisited: What can we learn from cytokines, CD classes and genes?" Anticancer Res, vol. 21, pp. 3653–3662, 2001.

[22] G. Krueger, G. Marshall, L. Buja, H. Schroeder, M. Brandt, G. Wang, and U. Junker, "Growth Factors, Cytokines, Chemokines and Neuropeptides in the Modeling of T-Cells," In Vivo, vol. 16, pp. 365–386, 2002.

[23] M. Burke, B. Morel, T. Oriss, J. Bray, S. McCarthy, and P. Morel, "Modeling the proliferative response of T-cells to IL-2 and IL-4," Cellular Immunol., vol. 178, pp. 42–52, 1997.

[24] A. Kirsch, An Introduction to the Mathematical Theory of Inverse Problems, Springer-Verlag, 1996.

[25] R. Mehr, A. Globerson, and A. Perelson, "Modeling positive and negative selection and differentiation processes in the thymus," J. Theor. Biol., vol. 175, pp. 103–126, 1995.

[26] R. Mehr, M. Fridkis-Harell, L. Abel, L. Segel, and A. Globerson, "Lymphocyte development in irradiated thymuses: Dynamics of colonization by progenitor cells and regeneration of resident cells," J. Theor. Biol., vol. 177, pp. 181–192, 1995.

[27] R. Mehr, A. Perelson, M. Fridkis-Harell, and A. Globerson, "Feedback regulation of T-cell development in the thymus," J. Theor. Biol., vol. 181, pp. 157–167, 1996.

[28] J. Mahaffy, J. Belair, and M. Mackey, "Hematopoietic model with moving boundary condition and state dependent delay: applications in erythropoiesis," J. Theor. Biol., vol. 190, pp. 135–146, 1998.

[29] B. Adkins, V. Charyulu, Q. Sun, D. Lobo, and D. Lopez, "Early block in maturation is associated with thymic involution in mammary tumor-bearing mice," J. Immunol., vol. 164, pp. 5635–5640, 2000.

[30] A. Abbas, Cellular and Molecular Immunology, Philadelphia: W. B. Saunders Company, 2000.

[31] J. McNamee, F. Stenger, and E. L. Whitney, "Whittaker's cardinal function in retrospect," Math. of Comp., vol. 25, pp. 141–154, 1971.

[32] W. Press, B. Flannery, S. Teukolsky, and W. Vetterling, Numerical Recipes, Cambridge University Press, Cambridge,1986.

[33] C. Penit, B. Lucas, and F. Vasseur, "Cell expansion and growth arrest phases during the transition from precursor ($CD4^-8^-$) to immature ($CD4^+8^+$) thymocytes in normal and genetically modified mice," J. Immunol., vol. 154, pp. 5103–5113, 1995.

[34] C. Penit, F. Vasseur, and M. Papiernik, "In vivo dynamics of $CD4^-8^-$ thymocytes: Proliferation, renewal and differentiation of different cell subsets studied by DNA biosynthetic labeling and surface antigen detection," Eur. J. Immunol., vol. 18, pp. 1343–1350, 1988.

[35] D. Godfrey, J. Kennedy, K. Suda, and A. Zlotnik, "A developmental pathway involving four phenotypically and functionally distinct subsets of $CD3^-CD4^-CD8^-$ triple negative adult mouse thymocytes defined by CD44 and CD25," J. Immunol., vol. 150, pp. 4244–4252, 1993.

[36] G. Krueger, M. Brandt, G. Wang, F. Berthold, and L. Buja, "A computational analysis of Canale-Smith syndrome: Chronic lymphadenopathy simulating malignant lymphoma," Anticancer Res, vol. 22, pp. 2365–2372, 2002.

[37] G. Krueger, M. Brandt, G. Wang, and L. Buja, "Dynamics of HTLV-1 leukemogenesis: Data acquisition for computer modeling," In Vivo, vol. 16, pp. 87–92, 2002.

Received on Mar. 28, 2004. Revised on Apr. 28, 2004.

E-mail address: Guanyu.Wang@uth.tmc.edu